



The Role of Pore Pressure on the Mechanical Behavior of Coal Under Undrained Cyclic Triaxial Loading

Chunlin Zhong^{1,2} · Zhenyu Zhang^{1,2} · P. G. Ranjith³ · Chengpeng Zhang² · Kangsheng Xue^{1,2}

Received: 19 April 2021 / Accepted: 1 November 2021 / Published online: 3 December 2021
© The Author(s), under exclusive licence to Springer-Verlag GmbH Austria, part of Springer Nature 2021

Abstract

Geofluids widely exist in natural rocks, and the fluid overpressure affects the mechanical behavior of rocks, triggering dynamic instability events. To investigate the role of pore fluid in low-permeability coal away from excavation boundary but still influenced by the periodic excavation disturbance, a series of undrained cyclic triaxial compressive tests were conducted on saturated coal. The results show that pore water has little effect on the axial strain evolution of coal, but has a significant effect on the radial and volumetric strain evolution. Different from dry coal, the saturated coal samples (except the coal samples SUC 1-1 and SUC 1-2 which show a slight volume shrinkage stage) show dilation deformation directly without any volume shrinkage, due to regional overpressure caused by the undrained condition. With this constraint against crack closure, a low frictional strength of crack surfaces was produced, favoring instability. Moreover, the saturated coal cracks cannot close tightly at the loading stage due to water propping effect, resulting in that the crack could not keep stationary, instead it slips throughout the loading and unloading processes. Also, the pore overpressure provides tensile stress, producing a large number of macro-tensile cracks in the final failure. This tensile cracking process is influenced by the loading frequency, as the pore pressure decay lags behind the unloaded stress, producing pore overpressure to tensile cracking in the unloading process. This lag effect becomes more prominent with the increase of cyclic loading frequency. Consequently, the number of tensile cracks of saturated coal at the loading frequency of 0.4 Hz is larger than that at the loading frequency of 0.1 Hz.

Highlights

- The pore overpressure promote the deformation growth to the direction of minimum principal stress.
- Dilatancy occurred directly from the start of loading for saturated coal due to regional overpressure.
- Pore overpressure provides tensile stress to the crack, producing a large number of macro tensile cracks in the final failure of the coal.
- The number of tensile cracks of saturated coal increased with the cyclic loading frequency due to the prominent lag effect of strain behind stress.

Keywords Pore pressure · Undrained cyclic loading · Saturated coal · Crack evolution

✉ Zhenyu Zhang
zyzhang@cqu.edu.cn

Chunlin Zhong
clzhong@cqu.edu.cn

P. G. Ranjith
Ranjith.Pathegama.Gamage@monash.edu

Chengpeng Zhang
lszcp1485@cqu.edu.cn

Kangsheng Xue
ksxue@cqu.edu.cn

¹ State Key Laboratory of Coal Mine Disaster Dynamics and Control, Chongqing University, Chongqing 400044, China

² Geofluids, Geomechanics and Geoenergy (3G) Research Group, Chongqing University, Chongqing 400044, China

³ Deep Earth Energy Laboratory, Department of Civil Engineering, Monash University, Building 60, Melbourne, VIC 3800, Australia

1 Introduction

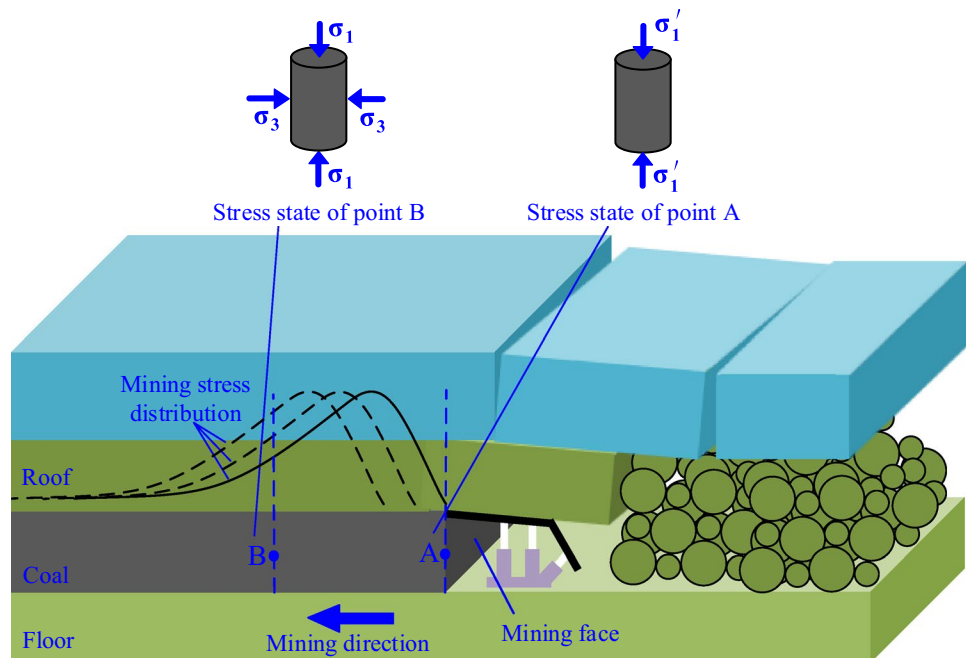
Geofluids widely exist in natural rocks, such as water, methane and carbon dioxide. The pore pressure formation and diffusion affect the mechanical behavior of rocks, and can be an unfavorable factor for geotechnical stability (Ferrero et al. 2010; Gatelier et al. 2002; Helmons et al. 2016). In underground coal mining, the mining excavation induces the stress redistribution (Li et al. 2003). With the coal cut, the vertical stress distribution in front of the excavation boundary evolves to the front coal periodically, producing cyclic stress disturbance to the coal in front of the mining face (Fig. 1). Furthermore, coal is a relatively soft sedimentary rock containing vulnerable vitrinite constituent and weak cleats, and its mechanical behavior is sensitive to engineering stress and fluid stress disturbance (Gao and Ghassemi 2017; Sakurovs et al. 2012; Vishal et al. 2015; Ye et al. 2017). It is fundamentally important to investigate the mechanical behavior of coal under the cyclic triaxial loading in mechanical model development for dynamic instability risk mitigation.

Water is an important factor weakening cohesive and frictional strength components of rocks (Kang et al. 2018; Liu et al. 2020; Tang 2018). Rock strength weakening can be caused by the clayey minerals swelling and softening (Cai et al. 2019; Vásárhelyi 2005; Wasantha and Ranjith 2014), causing geological and engineering instability events in rock engineering (Bai et al. 2013; Miao et al. 2018). However, such water-weakening effect on rock strength is not obvious and can be negligible for rocks with no or extremely low clayey constituents (Reviron et al. 2009). Alternatively,

pore water pressure can be developed within rocks, and the regional overpressure or pressure diffusion can significantly influence the physical structure and mechanical behavior of rocks, such as porosity change (Huang et al. 2016; Leclère et al. 2016; Tan et al. 2017), crack propagation and deformation process (Alvarez, et al. 2015; Bidgoli and Jing 2015; Roshan and Rahman 2011; Tang et al. 2018). Additionally, pore and interstitial gases frequently exist in the geological field, such as coal seam methane and carbon dioxide. Under compression, high pore pressure can be formed within rocks, and can trigger dynamic instability events (Castelletto et al. 2013; Elst et al. 2013; Hardebeck and Hauksson 1999; Robert et al. 1976). The dynamic instability events usually include disaster gestation, development, occurrence and stop in time sequence. For disaster mitigation, it is crucial to investigate the mechanical behavior of saturated or gassy coal under the quasistatic cyclic loading, where the role of pore fluid plays in the mechanical behavior of coal under cyclic triaxial loading is the core question.

Besides, the vertical stress distribution and stress state of unmined coal away from excavation boundary (such as Fig. 1, point B) are different from that near the excavation boundary (such as Fig. 1, point A). Therefore, the influence of pore pressure on points A and B are different. In our previous work, the pore water pressure effect on the mechanical properties of coal in the vicinity of unmined coal wall was investigated by conducting the drained uniaxial cyclic loading tests on the saturated coal (Zhong et al. 2019). It was found that in the vicinity of the excavation boundary, the pore fluid can easily be discharged through the well-interconnected pores and cracks during the loading

Fig. 1 Schematic illustration of mining stress distribution in longwall coal mining method



stage. The discharged pore fluid leads to the shrinkage of the pore volume in rock. However, the compression on the tight or low-permeability rocks promote the high pore fluid pressure development. For example, in the field away from the excavation boundary, the rock is in a three-dimensional stress state and the pore fluid is hard to be discharged in time when the rock is subjected to triaxial compression, especially in the low-permeability zone (French and Zhu 2017; Leclère et al. 2018; Lei et al. 2011). Therefore, the mechanical behavior of coal in the presence of pore fluid can vary at different distances away from boundary walls under cyclic loading. Furthermore, the formation or diffusion of pore overpressure is related to the duration of loading and unloading. Therefore, the influence of frequency of cyclic loading on pore pressure change cannot be ignored.

To investigate the role of pore pressure plays in coal in the dynamic disaster gestation stage, a series of cyclic triaxial tests was carried out on dry and saturated coal under undrained conditions by considering different loading frequency, cycles and stress levels. The undrained pore fluid condition is applied to simulate pore pressure evolution process of coal far away from mining face. First, the evolution of mechanical properties of coal was analyzed, and then the mechanism of pore pressure formation and the induced pore and crack evolution were further discussed. For comparison purposes, a group of dry coal samples was used in the cyclic loading test to cast insights for dynamic instability mechanism in presence of geofluids.

2 Materials and Methods

2.1 Sample Preparation

The coal blocks were collected from No. 4 coal seam in Tingnan coal mine, Shaanxi province, northwest of China. The sampling location is shown in Fig. 2a. The buried depth of No. 4 coal seam is 401.32–788.60 m and the inclination angle of coal seam is 3°–7°. The proximate analysis shows that the coal contains 50.87% fixed carbon (C_{fx}), 16.15% ash (A_{ad}), 32.98% volatile matter (V_{daf}), and 4.63% moisture (M). The coal samples were drilled from coal blocks along the direction perpendicular to the horizontal stratification to be 50 mm in diameter as shown in Fig. 2b. According to the suggested standard of International Society of Rock Mechanics and Rock Engineering (Kim et al. 1999), the height to diameter ratio of cylindrical coal samples was 2:1, and two ends of each cylindrical coal samples were polished to be parallel within an accuracy of ± 0.02 mm. The finalized coal samples and their numbering are shown in Fig. 2c, in which the coal samples from SCT 1 to SCT 3 are used for triaxial compressive strength tests with saturated condition, the coal samples from DCT 1 to DCT 3 were used

for triaxial compressive strength tests under dry condition, while the rest of eight samples (SUC 1-1, SUC 1-2, SUC 2-1, SUC 2-2, SUC 3-1, SUC 3-2, DUC 2-1, DUC 2-2) were used for a series of cyclic triaxial loading tests.

2.2 Experimental Apparatus

The Geotechnical Consulting & Testing System (GCTS) was used for the triaxial loading tests as shown in Fig. 3. It mainly consists of a control module, loading module and data acquisition module. This equipment is capable of performing uniaxial and triaxial compressive experiments with axial loading up to 3000 kN. Silicon oil is used as the confining medium in the triaxial cell with a loading confinement capacity of 210 MPa. The pressure transducers are used to monitor the confining stress with an accuracy of 0.01 MPa. The linear variable differential transducers (LVTDs) were used to measure the axial and radial deformation with 6 mm range as shown in Fig. 3b. This equipment can perform a variety of loading modes, such as stress-controlled test mode and strain-controlled test mode. In this study, the stress-controlled test mode was adopted to simulate the periodical evolution of the support pressure in front of the mining face causing by continuous coal excavation.

The coal samples (except DUC 2-1 and DUC 2-2,) were saturated using the ZYB-II vacuum pressure saturation device as shown in Fig. 4a. It mainly consists of a vacuum unit, sample chamber, hydraulic pump, pressure gauges, and control valves. First, the coal samples were placed in the pressurization chamber. Then the chamber was deaired for one hour. Subsequently, water was injected into the chamber. A hydraulic pump was used to pressurize the water to 5 MPa and maintained for 5 h. Generally, the water-weakening effect of rocks also related to the saturated time (Tang et al. 2018). Therefore, it is necessary to reduce the saturation time to focus on the pore pressure effect on the coal. Figure 4b shows the time required for coal sample to be fully saturated under the atmospheric saturation and pressurize saturation condition. The water was pressurized to 5 MPa in the pressurize saturation condition. It can be seen that the coal sample was completely saturated in 5 h under the water pressure of 5 MPa, while in the atmospheric condition, it takes at least 80 h for the coal sample to be fully saturated. Therefore, the coal samples were saturated in the pressurized chamber here to ensure that the coal sample can be fully saturated in a short time and prevent strengthening weakens by water due to a long saturation time.

2.3 Test Procedure

Prior to the cyclic loading tests, the conventional triaxial compression tests were carried out to achieve the triaxial

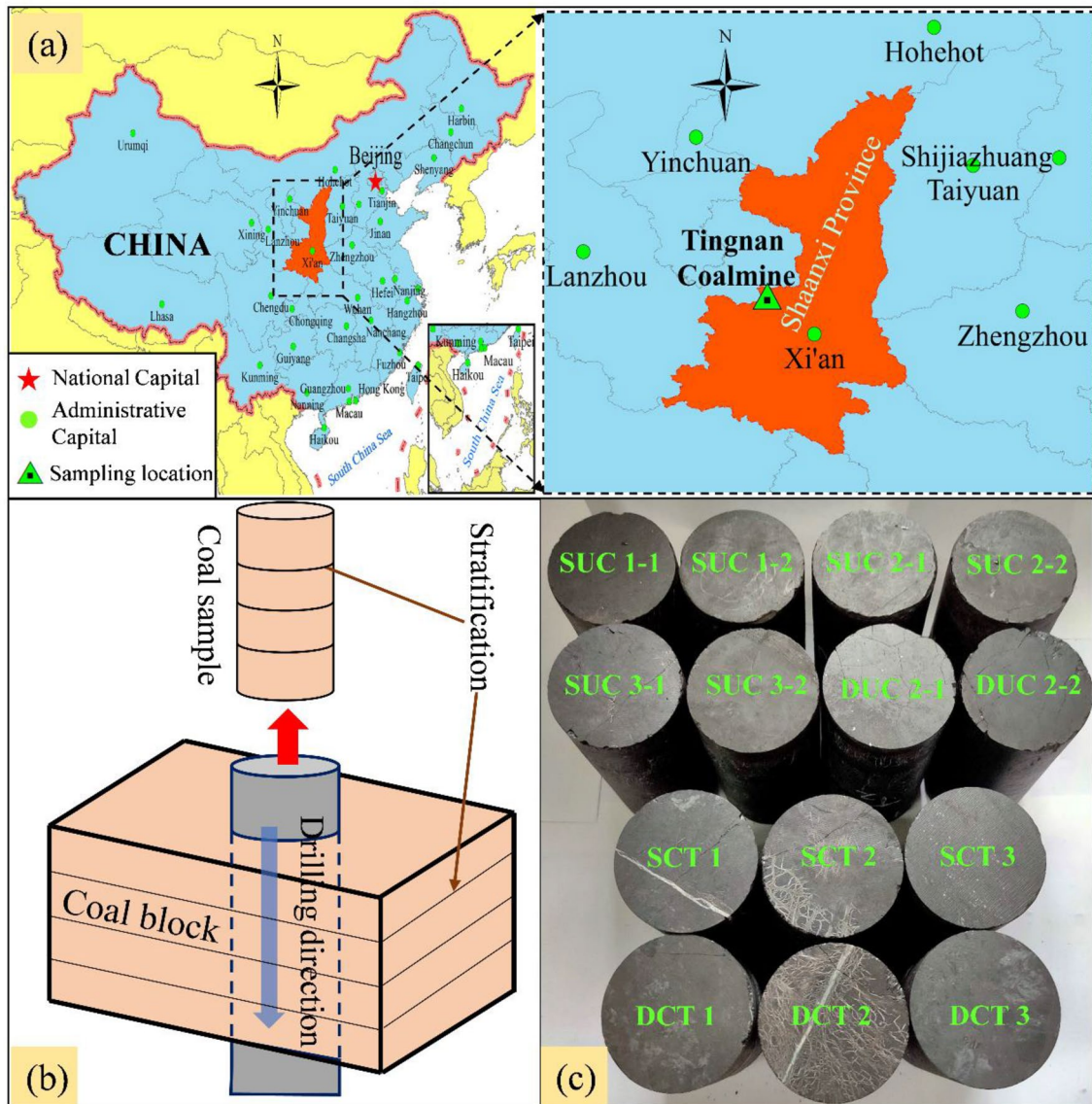


Fig. 2 The origin of selected coal and the standard coal samples

compression strength of coal. The confining stress was set as 8 MPa to simulate the stress state of coal at the in situ depth. Six coal samples, three dry and three saturated coal samples, were used for monotonic triaxial compression tests. The triaxial compression strength (σ_{ST}) of saturated coal is 68 MPa, while triaxial compression strength of dry coal sample (σ_{DT}) is 74 MPa on average.

Prior to the triaxial tests, coal sample was wrapped by the soft silicon rubber in case of confining oil leakage into the sample. Then the coal sample was mounted in the triaxial cell. The axial and radial deformation measurement devices were attached to the coal sample surface as shown in Fig. 3b. Then the triaxial cell was assembled up to prefill the confining silicone oil.

Figure 5 shows the loading procedure in the test. It can be seen that the entire loading process consists of three loading stages, loading stage 1, loading stage 2 and loading stage 3. In loading stage 1, the required confining stress is applied to the coal sample. At the start, $\sigma_1 = \sigma_2 = \sigma_3 = 0$. Then, the stresses of σ_1 , σ_2 and σ_3 were applied simultaneously to 8 MPa at a constant rate of 0.1 MPa/s. In loading stage 2, the confining stress is maintained invariable at 8 MPa, and the axial stress was continually increased at a constant rate of 0.1 MPa/s until it reaches the average stress level σ_{avr} (point B in Fig. 5). In loading stage 3, the axial cyclic loading program started from σ_{avr} until the failure of coal sample while keeping the confining stress at 8 MPa. The cyclic loading program will be stopped if the

Fig. 3 The geotechnical consulting and testing system

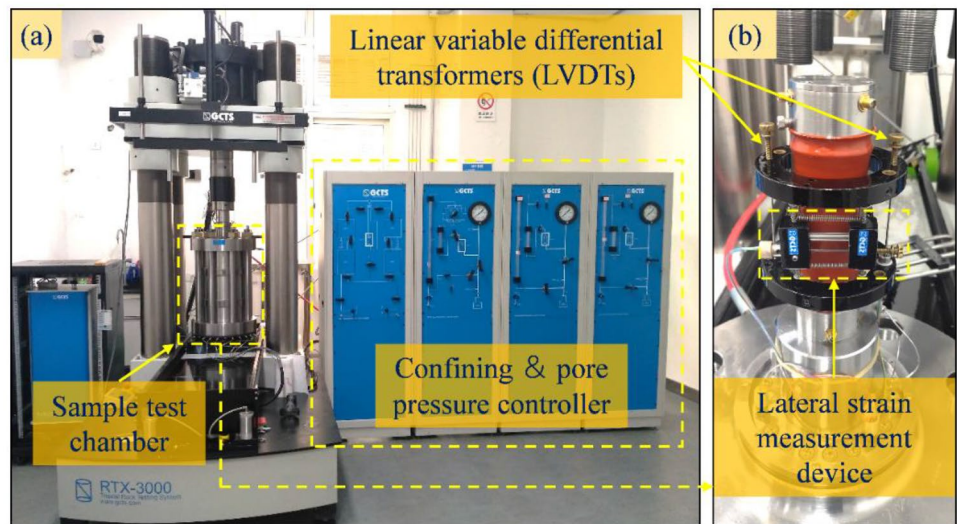


Fig. 4 **a** The ZYB-II vacuum pressure saturation device; **b** the average water absorption ratio of coal samples in atmospheric and pressurize saturate condition

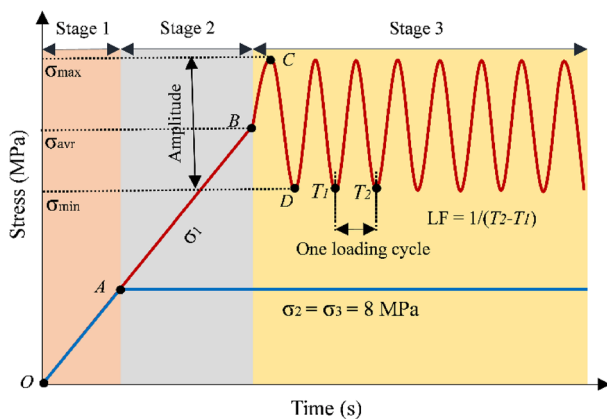
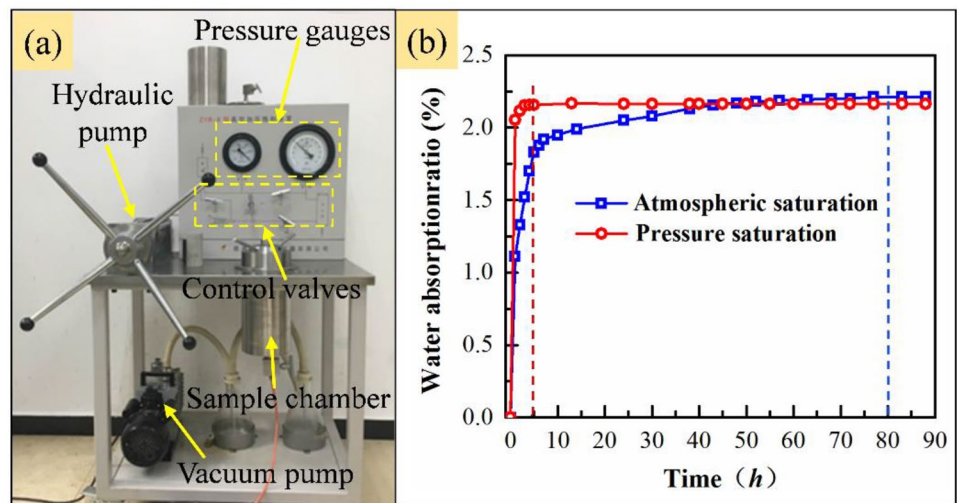


Fig. 5 Illustration of the loading test procedure in this experimental

increment of axial strain $< 0.001\%$ in 100 loading cycles because the coal sample has been fully compacted and cannot be damaged in this loading condition. The loading amplitude, frequency and loading cycles of coal samples in this test are summarized in Table 1. The formation or diffusion of pore overpressure is sensitive to loading and unloading rates. Therefore, to investigate the mechanical role of the pore fluid plays in the gestation stage of coal dynamic disaster under loading and unloading rates, different loading frequencies (0.1 Hz and 0.4 Hz) were set up in the cyclic loading tests.

Table 1 The specific loading scheme for each coal sample in the cyclic loading tests

| Sample no. | Average stress level (σ_{avr}) | Amplitude | Loading frequency (LF) | Loading cycles |
|------------|---|------------------|------------------------|----------------|
| SUC1-1 | $0.5\sigma_{ST}$ | $0.4\sigma_{ST}$ | 0.1 Hz | 560 |
| SUC1-2 | $0.5\sigma_{ST}$ | $0.4\sigma_{ST}$ | 0.4 Hz | 700 |
| SUC2-1 | $0.6\sigma_{ST}$ | $0.4\sigma_{ST}$ | 0.1 Hz | 4 |
| SUC2-2 | $0.6\sigma_{ST}$ | $0.4\sigma_{ST}$ | 0.4 Hz | 1000 |
| SUC3-1 | $0.7\sigma_{ST}$ | $0.4\sigma_{ST}$ | 0.1 Hz | 200 |
| SUC3-2 | $0.7\sigma_{ST}$ | $0.4\sigma_{ST}$ | 0.4 Hz | 580 |
| DUC2-1 | $0.6\sigma_{DT}$ | $0.4\sigma_{DT}$ | 0.1 Hz | 330 |
| DUC2-2 | $0.6\sigma_{DT}$ | $0.4\sigma_{DT}$ | 0.4 Hz | 650 |

Note: σ_{ST} is the triaxial compression strength of saturated coal with confining pressure 8 MPa; σ_{DT} is the triaxial compression strength of dry coal with confining pressure 8 MPa

3 Results

3.1 Mechanical Properties of Coal

Figure 6a shows the deviatoric stress–axial strain curves of coal samples in the monotonic triaxial compressive tests, and Table 2 lists the triaxial compressive strength (TCS), Poisson's ratio and Young's modulus. Figure 6a shows that there is no obvious difference in the axial stress–strain curve profiles between saturated and dry coal sample. The averaged triaxial compressive strength of saturated coal is slightly lower than that of dry coal with 14.8% strength reduction, but the Young's modulus of saturated increased by approximately 2.03%. As a consequence, the peak axial strain of saturated coal is generally smaller than that of dry coal, indicating that the triaxial compressive strength and deformability prior to peak strength of saturated coal is reduced by the pore water. This is different from mechanical

Table 2 The mechanical properties of coal samples

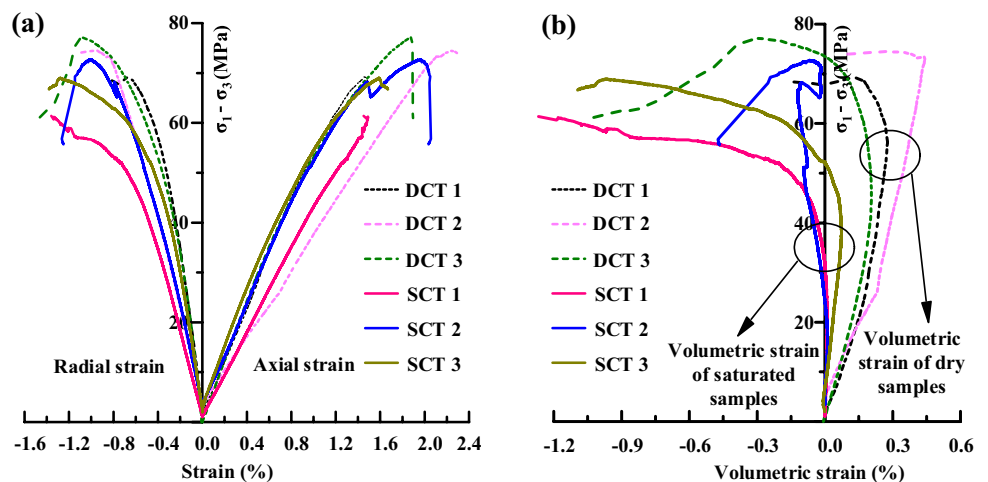
| Sample no. | TCS (MPa) | Poisson's ratio (ν) | Young's modulus (GPa) |
|---------------|-----------|---------------------------|-----------------------|
| DT1 | 70 | 0.29 | 5.65 |
| DT2 | 75 | 0.37 | 3.84 |
| DT3 | 77 | 0.36 | 5.28 |
| Average value | 74 | 0.34 | 4.92 |
| ST1 | 61 | 0.47 | 4.31 |
| ST2 | 73 | 0.45 | 5.43 |
| ST3 | 69 | 0.44 | 5.33 |
| Average value | 68 | 0.45 | 5.02 |

behavior of saturated coal by immersing the coal sample in water for a long time, where the strength and Young's modulus reduce with an increase in the peak axial strain (Helmons et al. 2016; Vishal et al. 2015). Such a difference can contribute to the effect of pore pressure caused by water inclusion, instead of solely water-weakening effect, confirming the validity of saturated coal sample preparation process for this study. It is also found that the Poisson's ratio of saturated coal increased by approximately 32.4% where the Poisson's ratio is calculated by the formula:

$$\nu = -\epsilon_r / \epsilon_a, \tag{1}$$

where ϵ_r is the radial strain in the elastic deformation section and ϵ_a is the axial strain in the elastic deformation section. As the evolution of axial strain tends to be not much different between saturated and dry coal samples, the main reason for the large difference in Poisson's ratio between saturated and dry coal samples can attribute to the difference in radial strain evolution. As shown in Fig. 6a, the radial strain of saturated coal samples greatly differs from that of dry coal samples in the loading process, where the saturated coal is

Fig. 6 The deviatoric stress–strain curves of coal samples in the monotonic triaxial compressive tests



much easier to dilate along the radial direction during the compressive loading process.

Figure 6b shows the deviatoric stress—volumetric strain curves of saturated and dry coal samples. A positive value in volumetric strain represents compression, while a negative value denotes volume dilatation. It can be found that the dry coal samples (dotted lines, DCT 1, DCT 2 and DCT 3) have an obvious compressive deformation stage, while saturated coal samples did not obvious volume compression, illustrating volume dilatation directly (solid lines, especially SCT 1 and SCT 2).

3.2 Stress–Strain Curves Under Cyclic Loading

Two dry and six saturated coal samples were used for the cyclic triaxial tests under different loading conditions. Figure 7 shows the deviatoric stress–strain curves of coal samples. Starting from the initial stress of $0.5\sigma_{ST}$, the saturated coal samples did not fail at loading frequencies of both 0.1 Hz and 0.4 Hz. When the initial stress increased to $0.6\sigma_{ST}$, the coal sample SUC 2-1 failed after four loading cycles at the frequency of 0.1 Hz, but did not fail at the loading frequency of 0.4 Hz (coal sample SUC 2-2). With the initial stress increased to $0.7\sigma_{ST}$, the saturated coal samples failed at the two loading frequencies. However, dry coal samples remained stable under the two loading frequencies during cyclic loading process with the initial stress of $0.6\sigma_{ST}$.

When the initial stress increased to $0.6\sigma_{ST}$ in loading stage 2, the axial strain of saturated coal samples (SUC 2-1 and SUC 2-2) are 0.979% and 0.654%, and the radial strain are -0.431% and -0.743% , respectively, while the axial strain of dry coal samples (DUC 2-1 and DUC 2-2) are 0.509% and 0.942% for the initial stress case of $0.6\sigma_{DT}$. The axial strain evolution of dry coal samples tends to be not much different from that of saturated coal. However, the radial strain of dry coal samples is -0.191% and -0.311% , much smaller than that of saturated coal samples.

For the cycling loading stage 3, the increment of axial and radial strains of saturated coal is obviously larger than that of dry coal during the cyclic triaxial loading by comparing Fig. 7a–f with Fig. 7g–h. For example, the increment of axial strain of saturated coal samples is 0.448% and radial strain 0.461% as shown in Fig. 7d, while those of the dry coal samples are 0.198% and 0.025%, respectively (Fig. 7h). Figure 7 also shows that the deviatoric stress–strain (axial and radial strain) curves and mechanical properties of coal samples were significantly influenced by the loading frequency. As shown in Fig. 7a and 7b, when the loading frequency is 0.1 Hz, the saturated coal sample SUC 1-1 was fully compacted within 560 loading cycles, while at the loading frequency of 0.4 Hz, the loading cycles of 700 was desired to reach the full compression state. The saturated coal sample SUC 3-1

failed after 200 loading cycles with the loading frequency of 0.1 Hz (Fig. 7e and f), but when the loading frequency increased to 0.4 Hz, the saturated coal sample SUC 3-2 failed after 580 loading cycles.

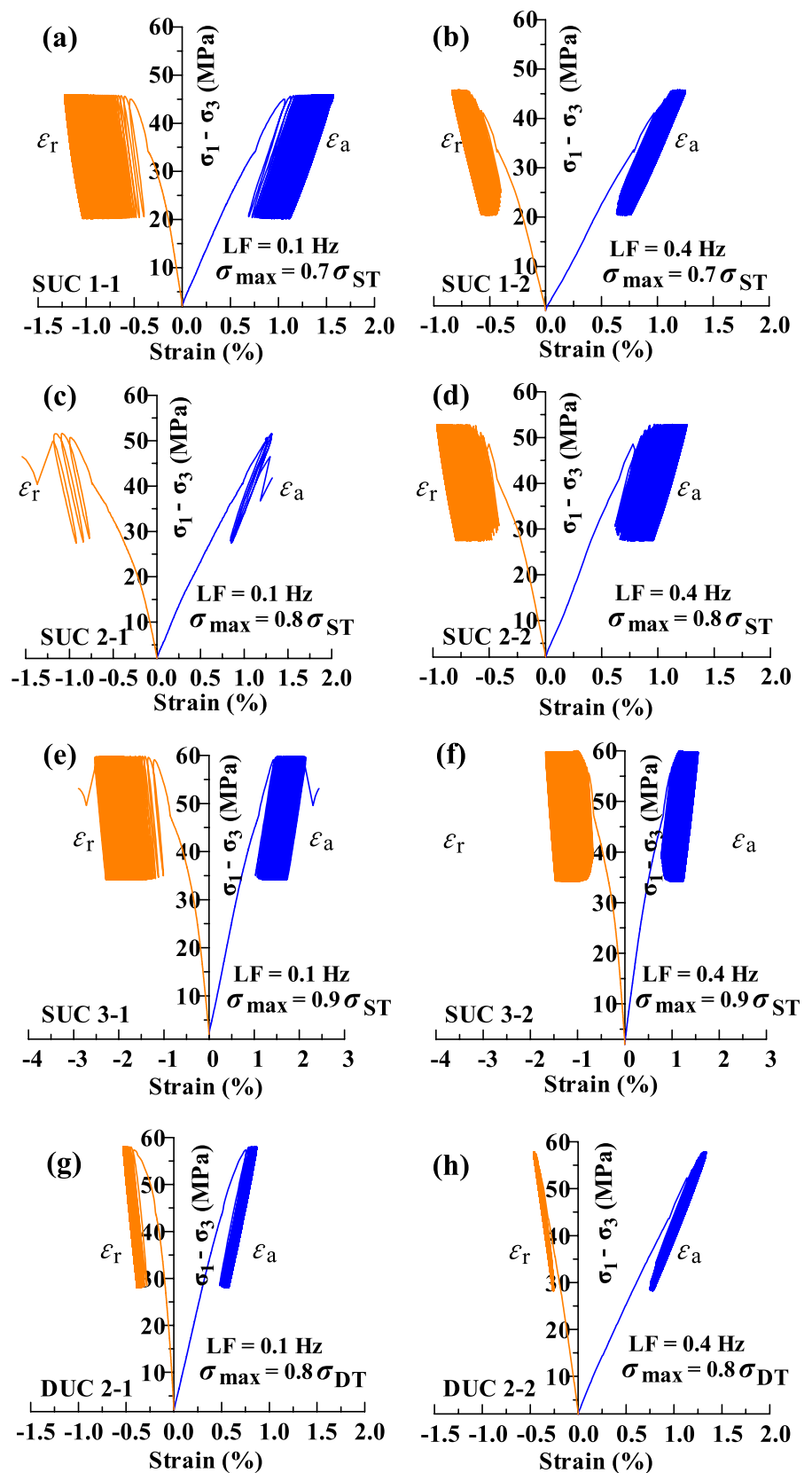
3.3 The Residual Strain and Maximum Strain Under Cyclic Loading

Figure 8 shows the residual strain of each loading cycle. The residual strain evolution can reflect the damage of coal samples caused by the cyclic loading. In Fig. 8, it can be seen that the residual strain (especially residual radial strain) of saturated coal samples was larger than that of dry coal samples, indicating that more damage was produced within saturated coal samples. For coal samples without macro-failure (SUC 1-1, SUC 1-2, SUC 2-2, DUC 2-1 and DUC 2-2), the increment of residual strain in the first loading cycle was larger than the rest of loading cycles. In the subsequent loading cycle, the increment of residual strain gradually decreased and eventually reduced to zero. However, the residual strain evolution of failed coal samples (SUC 2-1, SUC 3-1 and SUC 3-2) can be divided into three stages. First, the increment of residual strain gradually decreased in the early cyclic loading stage. Then the increment of residual strain almost maintained invariable. At this stage, the strain increased uniformly and the microcracks gradually developed within the coal samples. Finally, the microcracks initiated, grew and coalesced into macro-fractures, where the residual strain increased dramatically until macro-failure.

Figure 8 shows that the residual strain in the first loading cycle was related to the maximum stress level (σ_{max}). For example, the residual axial strain coal samples of SUC 1-2, SUC 2-2 and SUC 3-2 in the first loading cycle, corresponding to σ_{max} of $0.7\sigma_{ST}$, $0.8\sigma_{ST}$ and $0.9\sigma_{ST}$ are 0.589%, 0.617% and 0.984%, respectively. Also, the residual radial strain in the first loading cycle is -0.363% , -0.411% and -0.671% , respectively. Figure 8 also shows that the residual axial and radial strain in the first loading cycle are 0.843% and -0.761% for the saturated coal sample SUC 2-1 when the σ_{max} is $0.8\sigma_{ST}$, but reduced to 0.481% and -0.283% for the dry coal sample DUC 2-1. Therefore, the increment of residual strain in the first loading cycle for the dry coal samples is smaller than that of the saturated coal samples.

Note that the loading frequency of coal samples SUC 1-1, SUC 2-1 and SUC 3-1 was 0.1 Hz, and that of coal samples SUC 1-2, SUC 2-2 and SUC 3-2 was 0.4 Hz. It is clear that the residual strain of the saturated coal samples in each loading cycle was related to the loading frequency. For example, it can be seen in Fig. 8 that the residual strain of coal samples SUC 3-1 at the loading frequency of 0.1 Hz was larger than that of coal sample SUC 3-2 at the loading frequency of 0.4 Hz in each loading cycle.

Fig. 7 Stress–strain curves of coal samples under various cyclic loading conditions: axial strain (ε_a); radial strain (ε_r); loading frequency (LF)



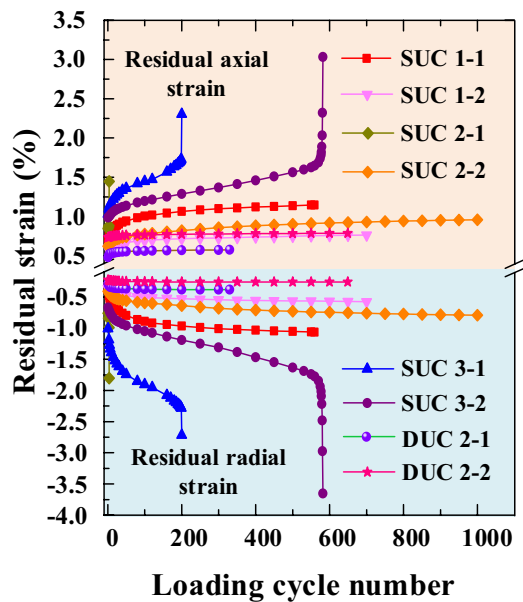


Fig. 8 The residual strain of saturated and dry coal samples during cyclic triaxial loading

3.4 The Volumetric Dilation Characteristics of Coal Under Cyclic Loading

Figure 9 shows the deviatoric stress—volumetric strain curves of all coal samples. During the cyclic triaxial loading, significant volumetric dilation occurred in the saturated coal and the ultimate volumetric strain increased with σ_{\max} . Compared with dry coal samples (Fig. 9g–h), the volumetric strain of saturated coal samples (Fig. 9a–f) was obviously larger. To further investigate the influence of pore water on the evolution of volumetric strain, the deviatoric stress–volumetric strain curve of saturated coal sample SUC 2-2 was compared with that of dry coal sample DUC 2-2, which has the same loading condition. The saturated coal sample SUC 2-2 showed a different evolution direction in volumetric strain with that of dry coal sample DUC 2-2 as shown in Fig. 9d and h. The volumetric strain of saturated coal sample SUC 2-2 was negative during the entire cyclic loading and unloading process, and the maximum volumetric strain was -0.658% after the cyclic loading, indicating that the coal sample SUC 2-2 was keeping in a dilatation state during cyclic loading test. However, the volumetric strain of dry coal sample DUC 2-2 was positive during the cyclic loading process and the maximum volumetric strain was 0.415% after the cyclic loading, showing that the volumetric of DUC 2-2 maintained a shrinking state during the cyclic triaxial test. In addition, Fig. 9 shows that the distribution of deviatoric stress–volumetric strain curves became intensified, and the increment of volumetric strain in each cycle decreases in the early several loading cycles as the loading frequency

increased from 0.1 Hz to 0.4 Hz, indicating that the significant role of loading frequency in controlling the volumetric strain development.

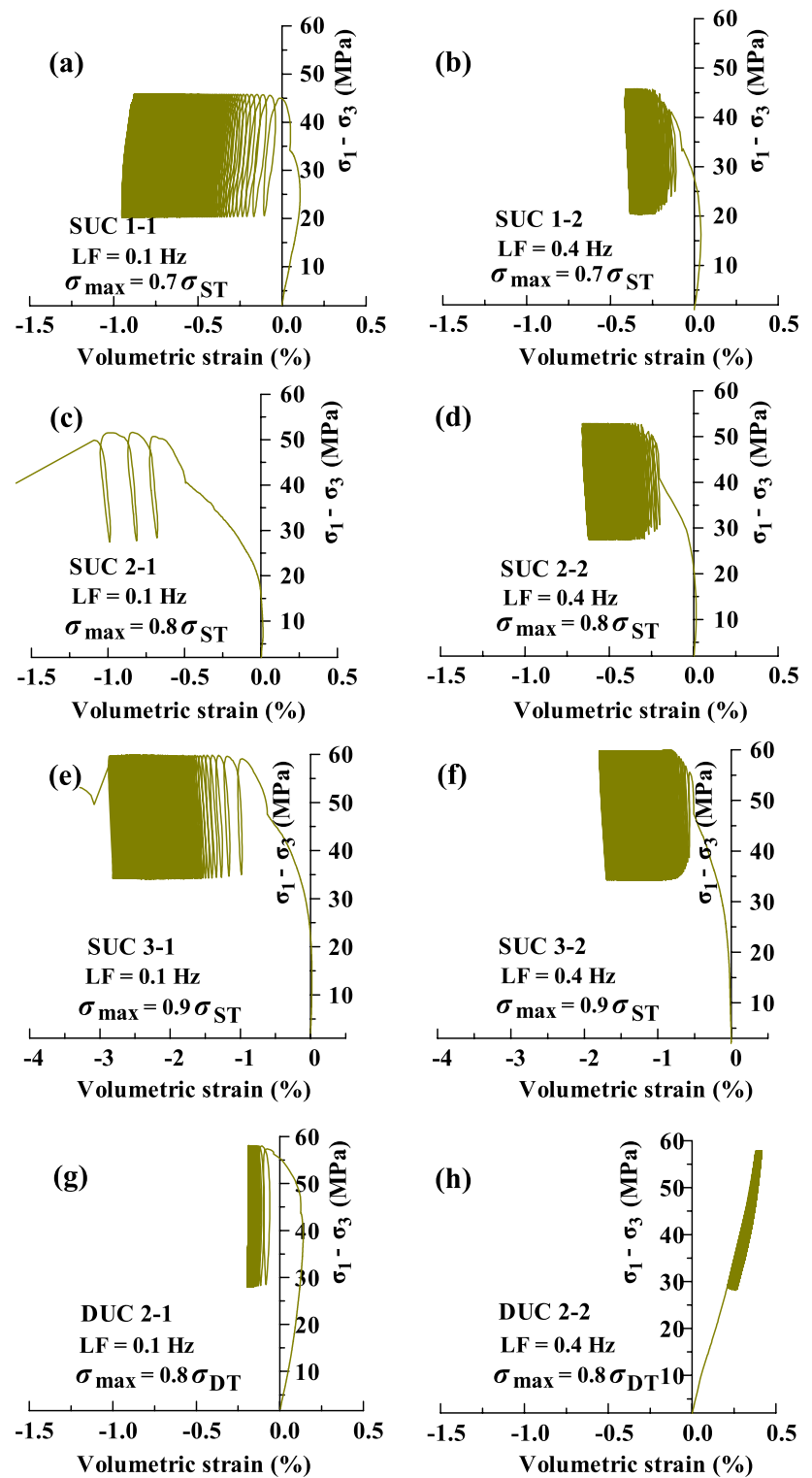
Figure 10 shows the deviatoric stress—volumetric strain curves of coal samples at the loading stage 2, in which the loading conditions are the same for all coal samples. The volumetric strain of dry coal samples (dotted lines) was positive, indicating that the volume of coal samples was compacted in loading stage 2. However, for the saturated coal samples (solid lines), the volumetric strain was negative (except SUC 1-1) during loading stage 2, indicating that volume expansion occurred in the saturated coal samples during the loading stage 2.

3.5 The Elastic Strain Evolution Characteristic Under Cyclic Loading

In the cyclic triaxial loading test, the strain increased in the loading process, and the strain decreased in the unloading process. However, in the initial stage of cyclic loading, the deformation would not completely recover when the load decreased to the minimum. The amount of strain that can be recovered strain is elastic strain, and the unrecovered strain component is defined as residual strain here. Clearly, the maximum strain consists of residual and elastic strain components as shown in Fig. 11. When the σ_{\max} has not exceeded the damage threshold of coal samples during the cyclic loading, the increment of residual strain and maximum strain in each loading cycle would gradually decrease to zero, forming a closed loop in the stress–strain curve with complete compression on coal samples and invariable residual and maximum strain. When the σ_{\max} exceeds the damage threshold of coal samples in the cyclic loading, the increment of residual strain experiences deceleration, steady and acceleration stages in sequence until ultimate failure. Figure 12 shows the elastic axial and radial strain evolution of coal samples. For coal samples without ultimate failure, the elastic strain increased in the initial loading stage and then kept almost invariable when being completely compacted. For coal samples with ultimate failure, the elastic strain decreased in the later loading stage and finally dropped to zero when the coal samples completely damaged. Figure 12 also shows that the increment of elastic strain for the loading frequency of 0.4 Hz was larger than that of loading frequency of 0.1 Hz in the initial loading stage.

In the early stage of cyclic loading, the closure of pre-existing pores and cracks in coal samples produced elastic deformation. With further cyclic loading, the amount of elastic strain gradually decreased. In the initial stage of cyclic loading, the increment of elastic strain due to the crack closure overweighed the reduced amount of elastic strain caused by the generation of the new cracks. Therefore, the elastic strain increased in the initial of cyclic

Fig. 9 The deviatoric stress–volumetric strain of coal samples in the cyclic loading test



loading stage. Figures 7 and 9 also show that the change of elastic strain is influenced by the cyclic loading frequency. It can be seen that the increment of residual strain (axial, radial and volumetric strain) was larger at the loading frequency of 0.1 Hz than that of 0.4 Hz in each cycle at the

early stage of cyclic loading. The reason is that the increment of elastic strain at the loading frequency of 0.4 Hz was larger than that of 0.1 Hz in the initial loading stage. This indicates that more severe damage occurred at the low loading frequency.

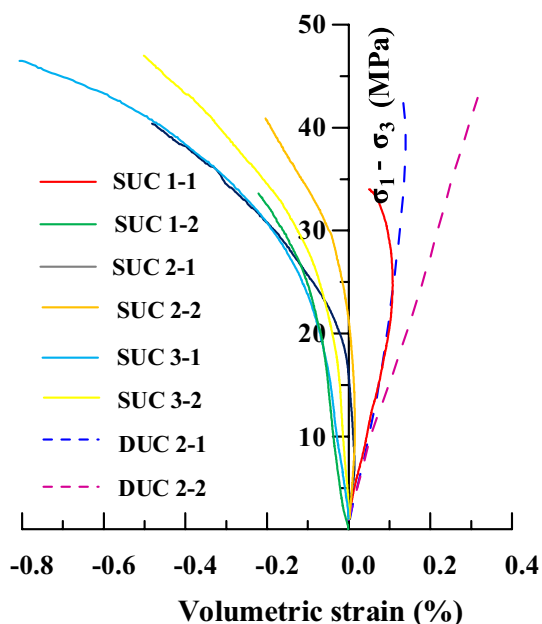


Fig. 10 The deviatoric stress–volumetric strain of coal samples during loading stage 2

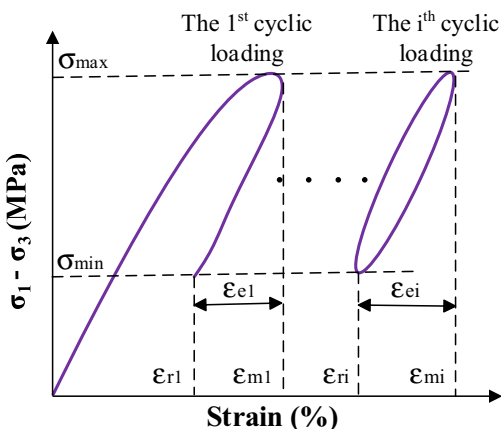


Fig. 11 The schematic illustration of residual, elastic and maximum strain in the cyclic loading: ϵ_{r1} , ϵ_{e1} and ϵ_{m1} represent the residual and elastic strain in the 1st cyclic loading, respectively; ϵ_{ri} , ϵ_{ei} and ϵ_{mi} represent the residual elastic and maximum strain in i th cyclic loading, respectively

4 Discussion

The pore pressure formation and its effect on the micro-/macro-crack propagation, radial strain and volumetric dilation were discussed in this section.

4.1 Pore Pressure Formation and Its Effect on Micro-crack Propagation

Figure 13 shows the deviatoric stress–strain curves of dry and saturated coal samples with 3rd, 300th and 650th loading cycles. As shown in Fig. 13a, the deviatoric stress–strain curves of dry coal sample (DUC 2-2) almost formed a closed loop in the 3rd loading cycle, and the deviatoric stress–strain curves gradually became the shape that the loading and unloading sections of deviatoric stress–strain curves gradually paralleled in 650th cycle. This indicates that Young's modulus of loading and unloading stages equals with cyclic loading. From the deviatoric stress–strain curves of 650th loading and unloading cycle, it can also be found that a stationary branch existed at the start of both loading and unloading processes. Interestingly, this stationary branch of loading is parallel with that of unloading stage as shown in Fig. 13a. The stationary branch that occurred in the deviatoric stress–strain curves of dry coal sample is due to the crack face does not slide. The Young's modulus in the loading and unloading stationary branch were defined as E_{LS} and E_{US} representing Young's modulus of crack without slide at the beginning of loading and unloading process (Minardi et al. 2018), while the Young's modulus of the crack slide in the loading is denoted by E_L and the one in unloading process is denoted by E_U . Therefore, the Young's modulus in the stationary branch (E_{LS} and E_{US}) is obviously different from E_L and E_U in the case of crack slide along two crack walls. Figure 13b shows that there is no stationary branch for the saturated coal sample at the initial stage of loading and unloading. Also, the saturated coal sample SUC 2-2 has a huge residual strain in the 3rd loading cycle when being compared with that of dry coal sample DUC 2-2 in Fig. 13a, and the area of hysteresis loop formed by the loading and unloading curves in the 365th loading cycle is larger than that of dry coal sample. The hysteresis loop in 365th tends to be fusiform and the loading and unloading curves are not parallel with each other anymore.

According to Fig. 13, the crack evolution processes of dry and saturated coal samples can be schematically shown in Fig. 14. For dry coal samples as shown in Fig. 14a, the open crack closes as the axial stress increases, but the closed cracks keep stationary as the accumulated shear stress along the crack surfaces is lower than the frictional resistance. However, crack slides once the accumulated shear stress exceeds the frictional resistance of crack surfaces. With further increase of axial loading, the crack propagates from the crack tips. In the subsequent unloading stage, the orientation of frictional resistance reverses due to the recovery of the previously developed elastic deformation. At the start of unloading process, cracks keep stationary as the shear stress is lower than the frictional resistance. With further decrease of axial stress, the crack slips but along the

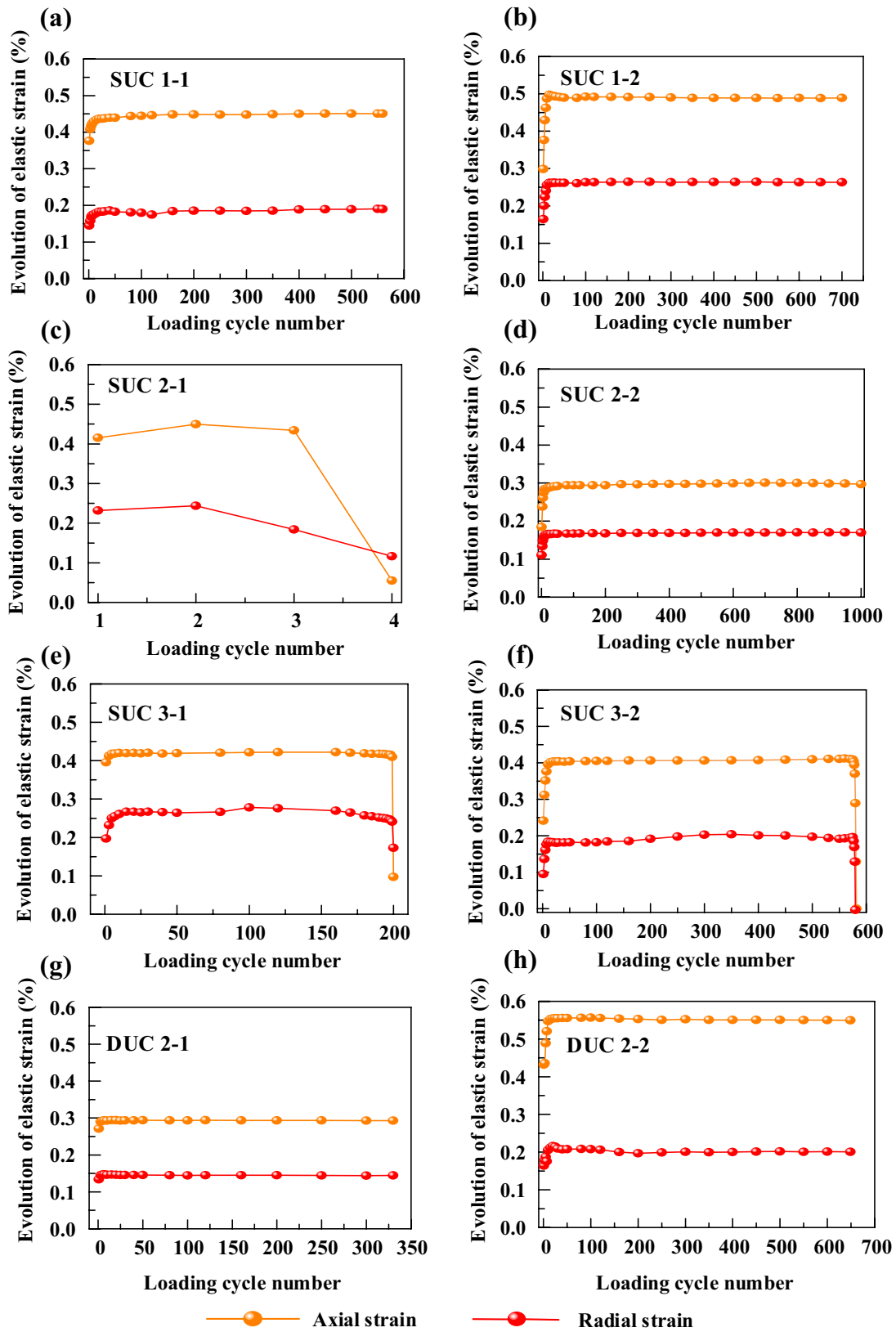
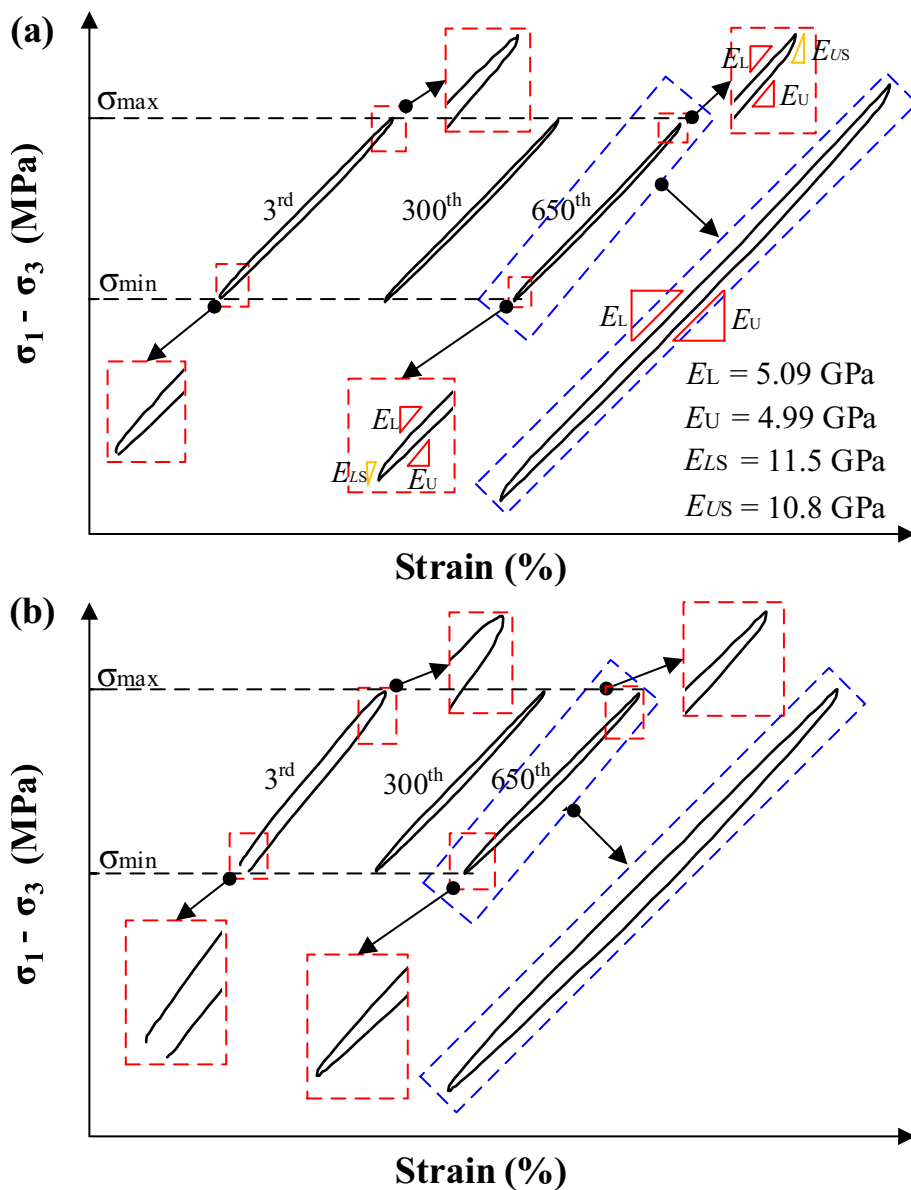


Fig. 12 The evolution of elastic strain for coal samples in the cyclic loading tests

Fig. 13 The deviatoric stress–strain curves of coal samples at 3rd, 300th and 650th loading cycles: **a** DUC 2-2; **b** SUC 2-2



direction opposite to that of loading process. Eventually, the elastic deformation of crack gradually recovers when the axial stress decreases to the minimum level. Such mechanical behavior of the crack repeats periodically during the cyclic loading and finally formed the stress–strain curve as shown in Fig. 13.

For saturated coal samples in Fig. 14b, the open crack is filled with water in the original state. In the loading stage, the crack tends to close when subjected to compressive loading, pressurizing the water in crack and accordingly building up high pore pressure. In the loading stage, the pore water pressure props up against the crack closure rendering low frictional resistance between two crack surfaces. On the other hand, the high pore pressure forms a tensile force in the crack tip, facilitating crack propagation. Therefore, the

formation of regional overpressure within cracks weakens the frictional strength of crack surfaces in the loading stage. In the unloading stage, the pore pressure gradually decreases due to the axial stress decrease and the deformed crack recovers to some extent. In the cyclic loading stage, the pore pressure increases and decreases periodically, which have a significant influence on the crack evolution and mechanical behavior of the coal samples. Compared with the cracking process of dry coal samples, the coal crack in the presence of pore/crack water cannot be compacted to close tightly in the loading stage, producing a lower frictional resistance between two crack surfaces. Therefore, the crack of saturated coal samples cannot keep stationary in the initial stage of loading and unloading and crack slip occurs throughout the loading and unloading process.

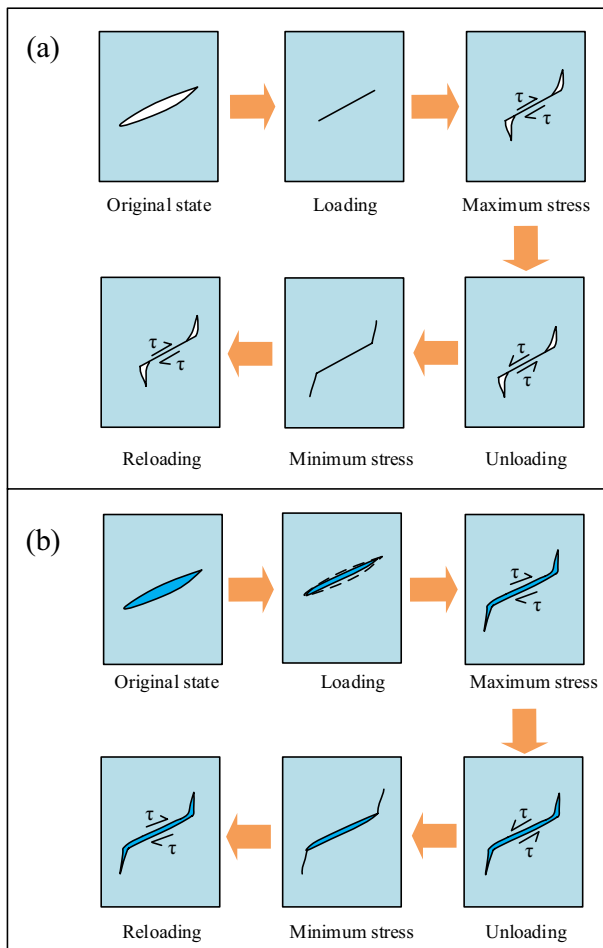


Fig. 14 Schematic illustration of crack evolution within coal samples: **a** dry coal sample; **b** saturated coal sample

4.2 Effect of Pore Pressure on Radial Strain Evolution During Cyclic Loading

Figure 15a shows the deviatoric stress–radial strain curve of saturated coal sample SUC 1-1 and Fig. 15b shows the residual radial strain evolution of all coal samples in terms of cycle number under cyclic triaxial loading condition. The maximum loading stress of coal sample SUC1-1 was $0.7 \sigma_{ST}$. It can be seen that the radial strain gradually increased during the cyclic loading and maintained as a constant when the coal sample was fully compacted. The increment of residual radial strain was largest in the first loading cycle, and with the increase of loading and unloading cycles, the increment of residual radial strain gradually decreased in each of subsequent loading cycle. The radial strain evolution of the undamaged coal samples is similar to the coal sample SUC 1-1, but for the failed coal samples, e.g. SUC 3-1 and SUC 3-2, the radial strain increased constantly throughout the cyclic loading process.

For comparison purpose, the results of radial strain evolution of coal under uniaxial (drained) cyclic loading condition (Fig. 16a and b) have been referred here (Zhong et al. 2019), where the drained uniaxial compressive condition is used to simulated the mechanical behavior of saturated coal in the vicinity of excavation boundary. Compared with the saturated coal under the drained uniaxial cyclic loading conditions, the saturated coal under the undrained cyclic triaxial loading conditions behaves distinctly. For saturated coal under the undrained cyclic triaxial loading condition, that is, the coal away from excavation boundary, the pore water cannot be discharged in time under compression and the pore pressure builds up due to the pore compression during the loading process. The pore pressure thus promotes the

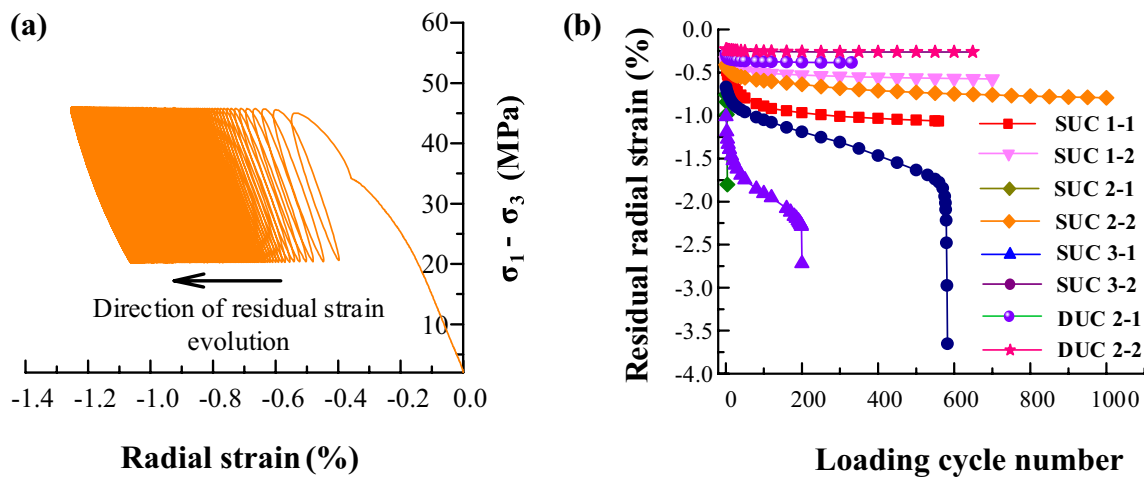


Fig. 15 The stress–radial strain curves and residual radial strain evolution of saturated coal samples under the undrained cyclic triaxial loading: **a** the stress–radial strain curve of saturated coal ample SUC

1-1; **b** the radial residual strain evolution of all coal samples under cyclic triaxial loading

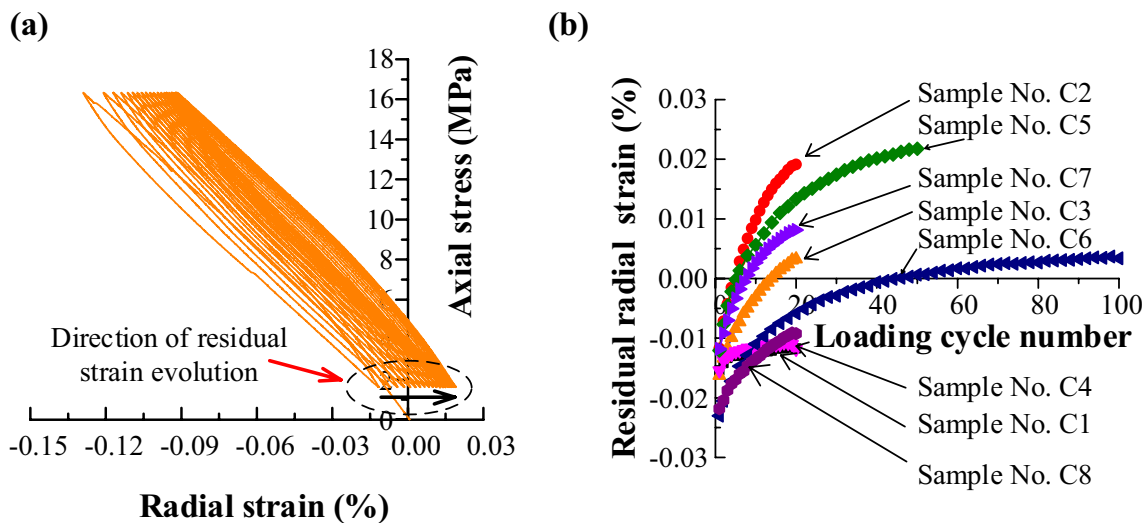


Fig. 16 The stress–radial strain curves and radial residual strain evolution of saturated coal samples under drained uniaxial cyclic loading: **a** the stress–radial strain curve of saturated coal sample C2; **b** the radial residual strain evolution of all saturated coal samples (Zhong et al. 2019)

crack generation and propagation during the cyclic triaxial loading and unloading process, leading to obvious dilatancy along the radial direction. For the saturated coal samples without failure, such as SUC 1-1, SUC 1-2 and SUC 2-2, the radial strain increases significantly in the early stage of cyclic loading due to pore overpressure. The crack density gradually increases and the water within the pre-existing pores or cracks is discharged into the new cracks in subsequent cyclic loading, resulting in pore water pressure decay and thus reducing the effect of pore water pressure on radial strain evolution described above. Therefore, the saturated coal samples SUC 1-1, SUC 1-2 and SUC 2-2 did not fail under the cyclic loading, although the increase of radial strain occur obviously in coal samples in the early stage of cyclic loading.

4.3 Effect of Pore Pressure on Volumetric Dilation During Cyclic Loading

Figures 6b, 9 and 10 show that the water within coal has a significant effect on the volumetric strain evolution characteristics of coal samples, where the dry coal samples demonstrated an obvious volume shrinkage phenomenon at the beginning of loading, while the saturated coal samples did not show volume shrinkage phenomenon during cyclic triaxial loading. The underlying mechanisms for the different volumetric strain evolution trends are explored here.

It is well known that the volumetric strain is contributed by axial and radial strains, and its calculation formula is

$$\epsilon_v = \epsilon_a + 2\epsilon_r, \tag{2}$$

where ϵ_v , ϵ_a and ϵ_r are the volumetric strain, axial strain and radial strain, respectively. As can be seen from Figs. 6 and 7, the axial strain evolution of dry coal samples tends to be not much different from that of saturated coal during the compression. Therefore, according to the calculation formula of volumetric strain, the volume deformation difference of dry and saturated coal is mainly sourced from radial deformation component. The coal is an organic porous medium of a wide range of pore and crack size distribution. For the dry coal samples, the pre-existing pores and cracks close in the initial loading stage, leading to shrinkage in volume. However, for the saturated coal samples, the pre-existing pores and cracks are filled with water and the water in the pores and cracks cannot be discharged in time under the undrained condition. When the coal sample is subjected to compressive loading, the pore and crack shrinkage occurs, building up high pore pressure and the developed pore pressure within pores and cracks resists against the pore and crack closure during the loading stage.

Furthermore, the pore pressure reduces the net stress and weakens the lateral confinement of coal. Figure 17 shows the scanning electron microscope (SEM) images of pores with different shape, distribution and connectivity within the saturated coal sample after cyclic loading test. Figure 17a and b illustrates the independent pores have poor interconnectivity with other pores. It can be seen that the pore has not closed after cyclic loading, but generated hydraulic tensile cracks derived from the pore wall instead. This is because during compression, the pore pressure continues to increase, exceeding the minimum principal stress (lateral confining pressure). The tensile cracks gradually develop under cyclic loading, finally forming macro-tensile cracks and promoting the deformation growth to the direction of minimum

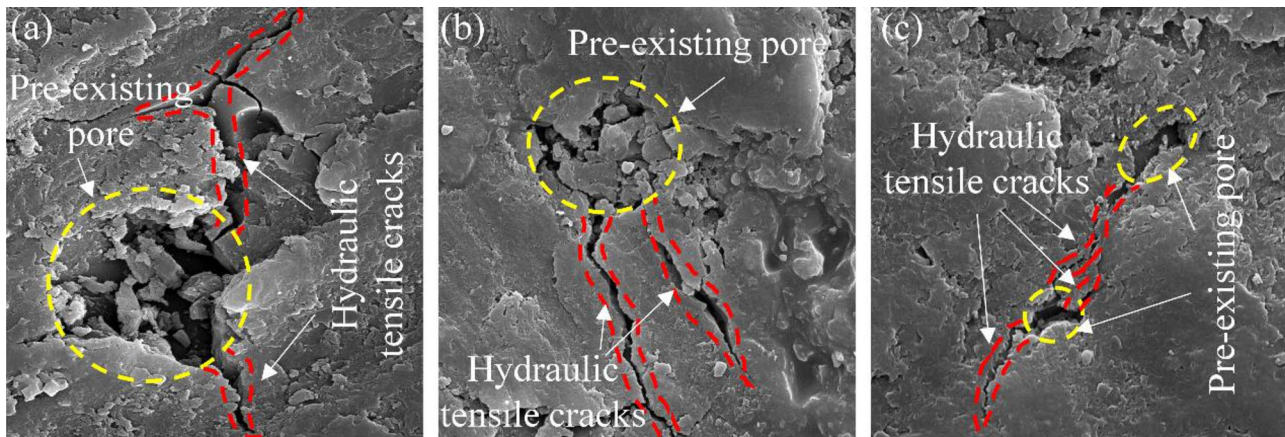


Fig. 17 The SEM images of pores inside the saturated coal sample after cyclic loading test

principal stress. Therefore, a large amount of radial strain develops within the saturated coal samples. The crack/pore as illustrated in Fig. 17c was oriented obliquely to the axial loading direction and such crack/pore would be closed in the loading stage in the dry coal samples. However, as shown in Fig. 17c, the presence of pore water hinders the closure of the cracks and leads to a reduction in the frictional strength of crack surfaces, favoring crack slip.

In summary, the results above show that the presence of pore water in coal not only makes the pre-existing pores unable to close, but also produces a large number of hydraulic cracks within coal due to the pore pressure, causing volumetric dilatancy of coal and resulting in an increase in pore and crack space. In addition, the newly developed cracks increases the permeability of coal, making the coal more conducive and facilitating the migration of surrounding fluids to new cracks, thereby forming a fluid-rich area. It is very likely to trigger a dynamic disaster in the subsequent cyclic of mining disturbances, especially when peak abutment stress moves to the fluid-rich area as shown in Fig. 1.

4.4 Effect of Pore Pressure on Macro-crack Evolution

Two coal samples (SUC3-1 and SUC 3-2) failed with many macro-cracks when σ_{\max} increase to $0.9\sigma_{ST}$. Therefore, the two failed coal samples were used to discuss the effect of pore pressure on macro-crack evolution. Figure 18 shows the macro-cracks of two failed coal samples (SUC3-1 and SUC 3-2), which were classified into tensile cracks (“T”) and shear cracks (“S”) (Cho et al. 2007; Yao et al. 2019). There were a large number of tensile cracks and almost no macro-shear cracks appeared in coal samples SUC 3-1 and SUC 3-2. Notably, the coal samples of SUC 3-1 and SUC 3-2 show obvious radial dilation deformation in the middle section of the coal sample. Moreover, the tensile cracks

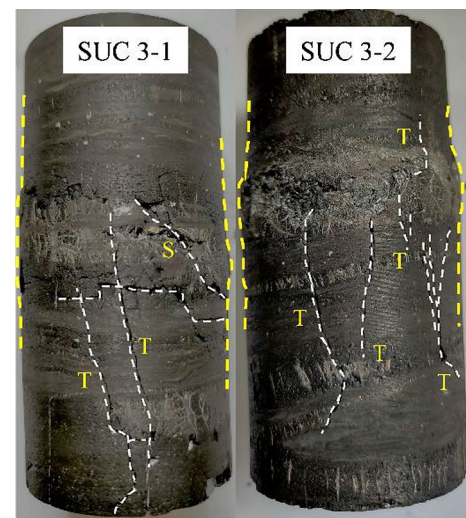


Fig. 18 Failure modes of saturated coal samples SUC3-1 and SUC 3-2

originated from the dilatancy position and propagated along the axial stress direction. The loading frequency of coal sample SUC 3-1 is 0.1 Hz, while the coal sample of SUC 3-2 is 0.4 Hz. Clearly, at the loading frequency of 0.1 Hz, the number of tensile cracks of coal sample is lower than that at the loading frequency of 0.4 Hz.

In the saturated coal samples, the pre-existing pores and cracks were filled with water. The shrinkage of pore and crack volume occurred in the loading stage, compacting pore water for pore pressure formation. The gradually increased pore pressure decreases the net stress and weakens the constraints along the radial direction, leading to the pore and crack evolution (Castelletto et al. 2013; Faulkner et al. 2018; Hillis 2000). The pore pressure also provides tensile stress to the pore and crack walls, producing tensile cracks (especially the cracks oriented parallel to the axial loading direction).

Moreover, under the triaxial loading, tensile stress, if exists, has the greatest possibility to distribute in the middle of the sample and near the boundary area of cylindrical sample (Yu et al. 2016). This is the reason why the deformation and tensile cracks firstly appeared in the middle of the samples. In general, the strain usually lags behind the stress in the cyclic loading for the rock material. In the loading stage, the water in pores was compacted, forming high pore pressure; in the subsequent unloading process, the elastic deformation recovered, but the strain recovery rate is slower than the unloading rate of stress, where pore pressure can exceed the external confining stress, forming pore overpressure and rotating the stress orientation. As a consequence, tensile cracks developed within coal. Such lag degree of recovered strain behind the stress unloading becomes more prominent with the frequency increase of loading and unloading (Mckavanagh and Stacey 1974; Song et al. 2019) Therefore, the number of tensile cracks of coal samples at loading frequency of 0.4 Hz were more than that of coal sample at the loading frequency of 0.1 Hz.

5 Conclusions

To investigate the role of fluids play in coal during the quasi-static stage of dynamic disaster gestation, a series of undrained cyclic triaxial loading tests were conducted on dry and saturated coal under the undrained conditions.

The results show that the pore pressure has little effect on the axial strain of coal samples, but has a significant effect on the radial and volumetric strain, indicating that the pore pressure can significantly weakens the lateral restraint effect. The dry coal samples have an obvious volumetric shrinkage process in the initial stage of cyclic loading, but the saturated coal samples have no volumetric compression phenomenon, demonstrating that the undrained condition facilitates the formation of regional high pressure in coal, favoring the crack slip and volumetric dilation. During the accelerated crack growth phase, the elastic strain gradually decreased. The radial and volumetric deformation of saturated are significantly larger than that of dry coal, which is contributed by undischarged pore water. The high pore pressure reduces the net confining stress of the coal samples, favoring radial deformation. Moreover, the pore pressure hinders the closure of cracks in the loading stage and reduces the friction resistance along the crack surfaces, causing crack slip and the volumetric dilation. The coal crack in the presence of water cannot be compacted to close tightly in the loading stage, producing a lower frictional resistance between two crack surfaces. As a result, the crack of saturated coal samples cannot keep stationary in the initial stage of loading and unloading and it slips throughout the loading and unloading process.

A large number of macro-tensile cracks appeared in the failed coal samples with pore water, as the pore pressure provides tensile force to the cracks and promotes the generation and propagation of tensile cracks. It is also found that this tensile cracking process is influenced by the loading frequency. The reason is that the pore pressure decay lags behind the stress unloading, forming pore overpressure for tensile crack development, and this lag effect becomes more prominent with the frequency increase of loading and unloading.

Acknowledgements This study was financially supported by the National Natural Science Foundation of China (Grant Nos. 51674047 and 51911530152) and the National Science Fund for Distinguished Young Scholars (Grant No. 51625401).

Author Contributions CZ: conceptualization, methodology, formal analysis, and writing—original draft; ZZ: conceptualization, methodology, and writing—review and editing; PGR: writing—review and editing; CZ: writing—review and editing; KX: methodology and writing.

Data Availability Not applicable.

Code Availability Not applicable.

Declarations

Conflict of interest The authors declare that they have no conflict of interest.

References

- Alvarez GM, Miedema SA, van de Ketterij RG, Yenigül NB, van Rhee C (2015) Effect of high hyperbaric pressure on rock cutting process. *Eng Geol* 196:24–36
- Bai H, Ma D, Chen Z (2013) Mechanical behavior of groundwater seepage in karst collapse pillars. *Eng Geol* 164:101–106
- Bidgoli MN, Jing L (2015) Water pressure effects on strength and deformability of fractured rocks under low confining pressures. *Rock Mech Rock Eng* 48:971–985
- Cai X, Zhou Z, Liu K, Du X, Zang H (2019) Water-weakening effects on the mechanical behavior of different rock types: phenomena and mechanisms. *Appl Sci* 9:4450
- Castelletto N, Ferronato M, Gambolati G, Janna C, Marzorati D, Teatini P (2013) Can natural fluid pore pressure be safely exceeded in storing gas underground? *Eng Geol* 153(2):35–44
- Cho N, Martin CD, Sego DC (2007) A clumped particle model for rock. *Int J Rock Mech Min Sci* 44(7):997–1010
- Elst N, Savage HM, Keranen KM, Abers GA (2013) Enhanced remote earthquake triggering at fluid-injection sites in the midwestern United States. *Science* 341:164–167
- Faulkner DR, Sanchez-Roa C, Boulton C, Hartog SD (2018) Pore fluid pressure development in compacting fault gouge in theory, experiments, and nature. *Int J Rock Mech Min Sci* 44(7):997–1010
- Ferrero AM, Migliazza M, Tebaldi G (2010) Development of a new experimental apparatus for the study of the mechanical behaviour of a rock discontinuity under monotonic and cyclic loads. *Rock Mech Rock Eng* 43:685–695

- French ME, Zhu W (2017) Slow fault propagation in serpentinite under conditions of high pore fluid pressure. *Earth Planet Sci Lett* 473:131–140
- Gao Q, Ghassemi A (2017) Pore pressure and stress distributions around a hydraulic fracture in heterogeneous rock. *Rock Mech Rock Eng* 473:131–140
- Gatelier N, Pellet F, Loret B (2002) Mechanical damage of an anisotropic rock under cyclic triaxial tests. *Int J Rock Mech Min Sci* 39:335–354
- Hardebeck JL, Hauksson E (1999) Role of fluids in faulting inferred from stress field signatures. *Science* 285:236–239
- Helmons R, Miedema SA, Grima MA, Rhee CV (2016) Modeling fluid pressure effects when cutting saturated rock. *Eng Geol* 211:50–60
- Hillis R (2000) Pore pressure/stress coupling and its implications for seismicity. *Explor Geophys* 31:448–454
- Huang Z, Jiang Z, Zhu S, Wu X, Yang L, Guan Y (2016) Influence of structure and water pressure on the hydraulic conductivity of the rock mass around underground excavations. *Eng Geol* 202:74–84
- Kang B, Jian L, Wei Z, Zheng X, Ni S, Liu Z (2018) Mechanical behavior and damage constitutive model of rock subjected to water-weakening effect and uniaxial loading. *Rock Mech Rock Eng* 52:97–106
- Kim K, Franklin JA, Bowling AJ, Lecomte P, Grob H (1999) International society for rock mechanics commission on testing methods. *Int J Rock Mech Min Sci Geomech Abstr* 24:53–73
- Leclère H, Faulkner D, Wheeler J, Mariani E (2016) Permeability control on transient slip weakening during gypsum dehydration: implications for earthquakes in subduction zones. *Earth Planet Sci Lett* 442:1–12
- Leclère H, Faulkner D, Llana-Fúnez S, Bedford J, Wheeler J (2018) Reaction fronts, permeability and fluid pressure development during dehydration reactions. *Earth Planet Sci Lett* 496:227–237
- Lei X, Tamagawa T, Tezuka K, Takahashi M (2011) Role of drainage conditions in deformation and fracture of porous rocks under triaxial compression in the laboratory. *Geophys Res Lett* 38:24310
- Li H, Ogawa Y, Shimada S (2003) Mechanism of methane flow through sheared coals and its role on methane recovery. *Fuel* 82:1271–1279
- Liu H, Zhu W, Yu Y, Xu T, Liu X (2020) Effect of water imbibition on uniaxial compression strength of sandstone. *Int J Rock Mech Min Sci*. <https://doi.org/10.1016/j.ijrmms.2019.104200>
- Mckavanagh B, Stacey F (1974) Mechanical hysteresis in rocks at low strain amplitudes and seismic frequencies. *Phys Earth Planet Inter* 8:246–250
- Miao F, Wu Y, Li L, Tang H, Li Y (2018) Centrifuge model test on the retrogressive landslide subjected to reservoir water level fluctuation. *Eng Geol* 245:169–179
- Minardi A, Ferrari A, Ewy R, Laloui L (2018) Nonlinear elastic response of partially saturated gas shales in uniaxial compression. *Rock Mech Rock Eng* 51(7):1967–1978
- Reviron N, Reuschlé T, Bernard JD (2009) The brittle deformation regime of water-saturated siliceous sandstones. *Geophys J Int* 178(3):1766–1778
- Roshan H, Rahman SS (2011) Analysis of pore pressure and stress distribution around a wellbore drilled in chemically active elastoplastic formations. *Rock Mech Rock Eng* 44:541–552
- Sakurovs R, He L, Melnichenko YB, Radlinski AP, Blach T, Lemmel H, Mildner D (2012) Pore size distribution and accessible pore size distribution in bituminous coals. *Int J Coal Geol* 100:51–64
- Song Z, Konietzky H, Fruehwirt T (2019) Hysteresis and dynamic response features of concrete exposed to repeated multilevel compressive loading. *J Mater Civ Eng*. [https://doi.org/10.1061/\(ASCE\)MT.1943-5533.0002703](https://doi.org/10.1061/(ASCE)MT.1943-5533.0002703)
- Tan QB, Zhang R, Gao MZ, Liu QY, Zhang ZT, Jia ZQ (2017) Coal permeability and crack distribution characteristics in unloading confining pressure experiments under different water pressures. *Therm Sci* 21(1):241–249
- Tang SB (2018) The effects of water on the strength of black sandstone in a brittle regime. *Eng Geol* 239:167–178
- Tang SB, Yu CY, Heap MJ, Chen PZ, Ren YG (2018) The influence of water saturation on the short- and long-term mechanical behavior of red sandstone. *Rock Mech Rock Eng* 51(9):2669–2687
- Vásárhelyi B (2005) Statistical analysis of the influence of water content on the strength of the miocene limestone. *Rock Mech Rock Eng* 38:69–76
- Vishal V, Ranjith PG, Singh TN (2015) An experimental investigation on behaviour of coal under fluid saturation, using acoustic emission. *J Nat Gas Sci Eng* 22:428–436
- Wasantha P, Ranjith PG (2014) Water-weakening behavior of Hawkesbury sandstone in brittle regime. *Eng Geol* 178:91–101
- Yao Q, Chen T, Tang C, Sedighi M, Huang Q (2019) Influence of moisture on crack propagation in coal and its failure modes. *Eng Geol*. <https://doi.org/10.1016/j.enggeo.2019.105156>
- Ye ZW, Zhang L, Hao DY, Zhang C, Wang C (2017) Experimental study on the response characteristics of coal permeability to pore pressure under loading and unloading conditions. *J Geophys Eng* 14(5):1020–1031
- Yerkes RF, Castle RO (1976) Seismicity and faulting attributable to fluid extraction. *Eng Geol* 10:151–167
- Yu B, Zhang Z, Kuang T, Liu J (2016) Stress changes and deformation monitoring of longwall coal pillars located in weak ground. *Rock Mech Rock Eng* 49(8):3293–3305
- Zhong C, Zhang Z, Ranjith PG, Lu Y, Choi X (2019) The role of pore water plays in coal under uniaxial cyclic loading. *Eng Geol*. <https://doi.org/10.1016/j.enggeo.2019.05.002>

Publisher's Note Springer Nature remains neutral with regard to jurisdictional claims in published maps and institutional affiliations.